Fryer, P., Pearce, J. A., Stokking, L. B., et al., 1992
Proceedings of the Ocean Drilling Program, Scientific Results, Vol. 125

37. BIOSTRATIGRAPHIC SUMMARY, LEG 125[1]

B. Stabell,[2] J. Ali,[3] G. Ciampo,[4] G. Milner,[5] Y.-J. Wang,[6] and Y. Xu[7]

ABSTRACT

Samples from 15 holes at nine sites in the Izu-Bonin–Mariana region were examined for calcareous nannofossils, foraminifers, diatoms, and radiolarians. The ages of the containing sediments range from middle Eocene to Holocene. Biostratigraphic indicators date the sediments flanking Conical Seamount in the Mariana forearc as Pleistocene, whereas sediments flanking a seamount at Site 784 in the Izu-Bonin forearc were dated as middle Miocene. Sediments in the Izu-Bonin forearc are as old as the middle Eocene. Useful magnetostratigraphic results range from Holocene to mid-Miocene. Nannofossils provided the most useful biostratigraphic framework, but were supplemented with satisfactory agreement by data from foraminifers, radiolarians, and diatoms. Evidence from the biostratigraphic framework shows the likely presence of a sedimentary hiatus in the early Miocene. The presence of a single short hiatus in the early Oligocene and two in the late Miocene and early Pliocene is suggested, but supporting evidence other than nannofossil data is sparse.

Evidence from approximate age-depth plots shows that sediment accumulation varies from hole to hole. The fastest rates of sediment accumulation were found to be in the late Miocene to Holocene whereas the slowest rates are present in the middle Eocene to Oligocene. The increased sedimentation rates in the late Miocene to Holocene resulted from an increase in volcanogenic sediment content from an uncertain source.

INTRODUCTION

During Leg 125 of the Ocean Drilling Program (ODP), Sites 778 through 786 were drilled in the Izu-Bonin–Mariana outer forearc region at depths between about 2660 and 4900 m (Fryer, Pearce, Stokking, et al., 1990) (Fig. 1). At Site 785, the hole was abandoned as a result of drilling problems after penetrating 104.7 m of Pleistocene pumice.

Eight holes at four sites near 19° 30′N, 146° 40′E were cored at Conical Seamount in the Mariana forearc (Fig. 1C). Sites 778 and 779 are situated halfway up the south and southeast flank of Conical Seamount at water depths of about 3900 m, and Site 780 is near the summit at a water depth of 3083 m. Site 781 is situated near the base of the seamount at a water depth of 4420 m.

Seven holes at five sites (Sites 782 through 786) were cored in the Izu-Bonin forearc near 31° N, 141° E at water depths between about 2660 and 4900 m (Fig. 1B). Sites 783 and 784 were cored on a seamount at water depths of 4649 and 4901 m, respectively. Holes 782A and 782B and Site 785 were cored on the outer margin of the Izu-Bonin forearc and are situated close together. Site 786 is situated in the same general area, but farther north.

We deal here with the more general aspects of the biostratigraphic results from Leg 125, discussed in detail in Ciampo (late Miocene to Holocene nannofossils), Milner (foraminifers), Stabell (diatoms), Wang (radiolarians), and Xu and Wise (middle Eocene to Miocene nannofossils) in this volume. Calcareous nannofossils occur at all sites (Fig. 2), but their presence depends on the water depth. Foraminifers are more sporadic, typically scarce, but show a similar distribution trend as that of the nannofossils. Siliceous microfossils are even more scarce than calcareous microfossils. The standard low-latitude calcareous nannofossil zonation of Okada and Bukry (1980) was used for the material discussed here. For Neogene planktonic foraminifers, the zonation of Blow (1969), as amended by Kennett and Srinivasan (1983) was used; for the Eocene/early Oligocene age sediments at Site 786, the tropical planktonic foraminiferal zonation of Berggren and Miller (1988) was used (discussed in Milner, this volume). The diatom zonation pro-posed by Barron (1985a, 1985b) for the equatorial Pacific, with the addition of the middle- to high-latitude zonations of Barron (1985b) and Akiba (1986), was used for diatoms, as discussed by Stabell (this volume). Radiolarian biostratigraphy followed the zonation of Sanfilippo et al. (1985), as discussed by Wang (this volume).

The nannofossil zonation of these holes is used in preference to the foraminiferal zonation because the nannofossils are generally better preserved and more common and include more age-diagnostic species. For Hole 784A, diatoms and radiolarians were used for zonation because of the lack of calcareous sediment. Magnetostratigraphic studies of these three holes (Ali et al., this volume) provided additional tie-points for calibrating age-depth relations.

Tables 1 through 3 summarize biostratigraphic and magnetostratigraphic studies and are based on data from Ali et al. (this volume), Ciampo (this volume), Milner (this volume), Stabell (this volume), Wang (this volume), and Xu and Wise (this volume).

RESULTS

Mariana Forearc–Conical Seamount Area

Four sites were drilled in the Conical Seamount area—778, 779, 780, and 781. The water depths range from 3000 to 4000 m. Sites 778, 779, and 780 at or near the crest of Conical Seamount encountered a thin sedimentary cover (maximum 30 m) that contains Pleistocene fossils. Nannofossil evidence confines these sediments to Zones CN14a to CN15, early to late Pleistocene (Fryer, Pearce, Stokking, et al., 1990). Site 781, however, near the base of the seamount, intersected a thicker microfossil-bearing sediment cover, with calcareous microfossils throughout the 247-m sediment column. Nannofossil evidence from Site 781 confines these sediments to Zones CN11b to CN15, early Pliocene to late Pleistocene. Foraminiferal data from

[1] Fryer, P., Pearce, J. A., Stokking, L. B., et al., 1992. *Proc. ODP, Sci. Results,* 125: College Station, TX (Ocean Drilling Program).
[2] Department of Geology, University of Oslo, P.O. Box 1047, Blindern, N-0316 Oslo 3, Norway.
[3] The Oceanography Department, The University, Southampton SO9 5NH, United Kingdom.
[4] Dipartimento Scienze della Terra-Largo, S. Marcellino 10, 1-80128 Napoli, Italy.
[5] Department of Geology, University of Western Australia, Nedlands, Western Australia 6009.
[6] Nanjing Institute of Geology and Paleontology, Academia Sinica, Chi-Ming-Ssu, Nanjing, People's Republic of China.
[7] Department of Geology, China University of Geosciences, Beijing 100083, People's Republic of China.

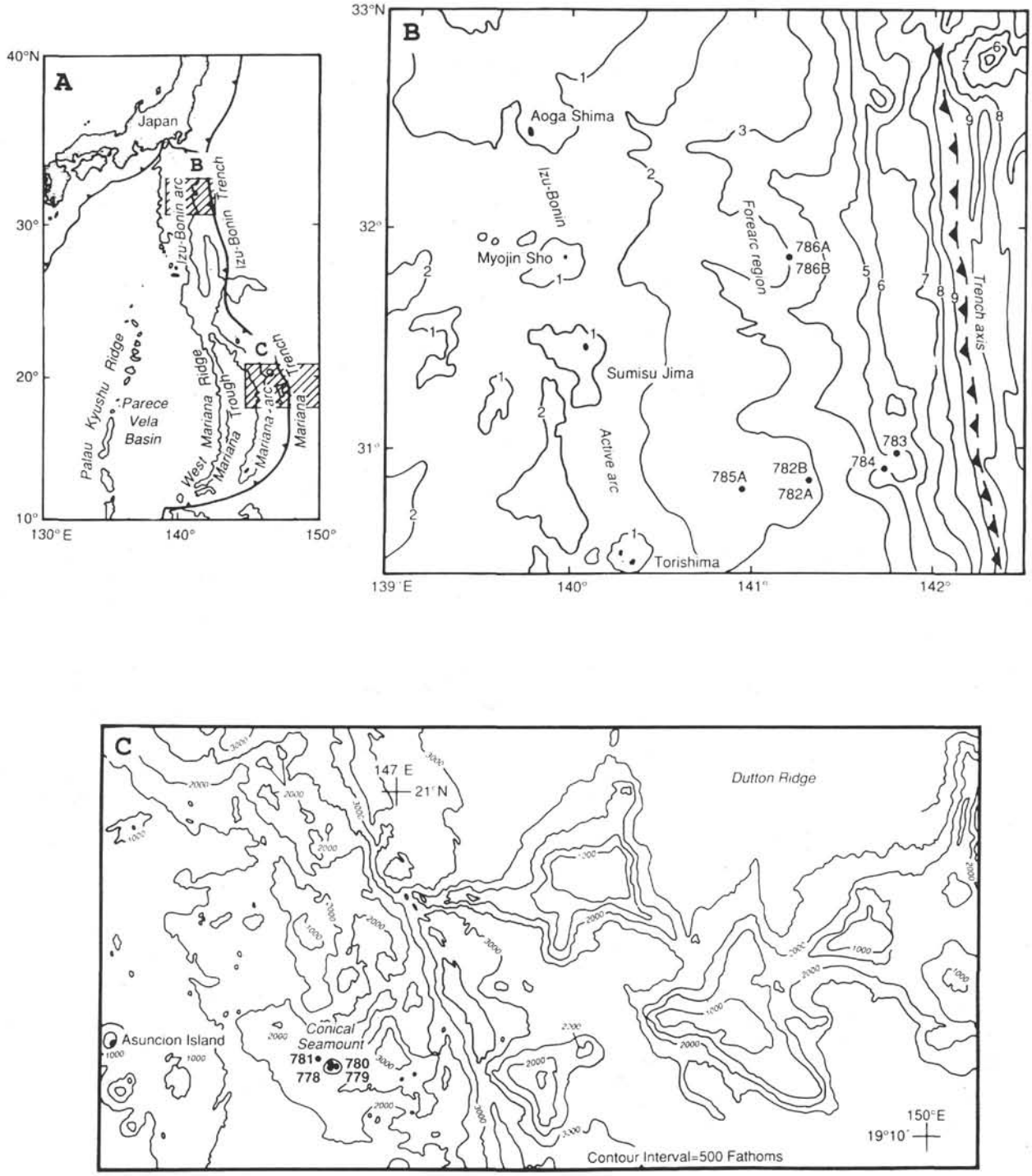

Figure 1. Investigated Leg 125 sites in the Izu-Bonin area. **A.** Regional setting. **B.** Precise setting of drill Sites 782–786. **C.** Transect across the Izu-Bonin region, showing the location of Sites 778–781.

each of the sites support these dates, whereas age-diagnostic diatom taxa were not observed (Fryer, Pearce, Stokking, et al., 1990).

Izu-Bonin Forearc

The sediments at Sites 783 and 784, at water depths below 4600 m, are thought to have been deposited near and below the carbonate compensation depth (Ciampo, this volume; Fryer, Pearce, Stokking, et al., 1990). These sites have few nannofossils and are barren of foraminifers, whereas siliceous microfossils (diatoms and radiolarians) occur. But at Site 783 the sediments could be dated only to the early Pliocene or older because of poor diatom and radiolarian preservation; Site 784 was dated to middle Miocene on the basis of radiolarian evidence (Wang, this volume).

Holes 782A and 786A could be dated to the middle Eocene nannofossil Zone CP13c (Xu and Wise, this volume). Foraminiferal data support these results. At Hole 786A, Milner (this volume) dated the basal sediments to planktonic foraminiferal Zone P10, early

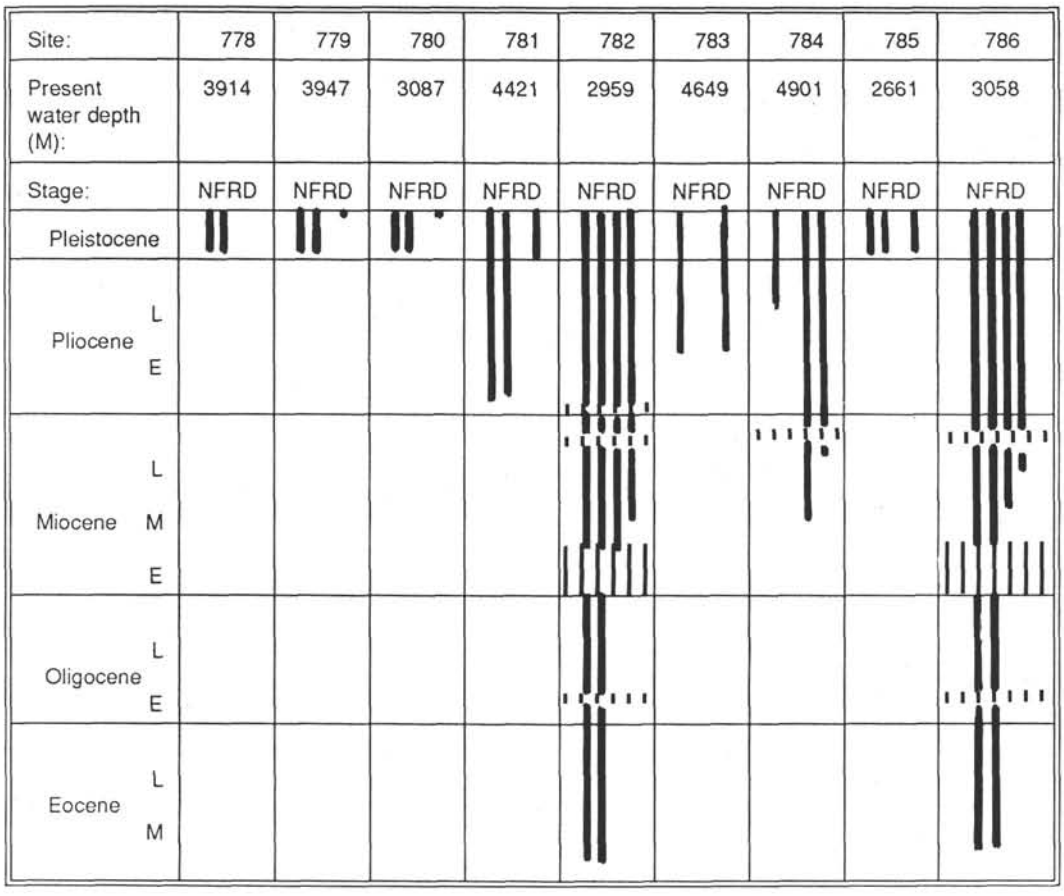

Figure 2. Occurrence of different microfossil groups at Leg 125 sites. N = calcareous nannofossils, F = foraminifers, D = diatoms, and R = radiolarians.

middle Eocene. Siliceous microfossils occur from the middle Miocene only at these sites. At Sites 782, 784, and 786 radiolarians occur at greater depths than diatoms (Fig. 2).

Magnetostratigraphic Results

Magnetostratigraphy for whole-core and discrete specimens from a transect of drill sites (782, 783, 784, and 786) across the Izu-Bonin forearc was integrated with the biostratigraphic data and correlated with the geomagnetic polarity time scale (see Ali et al., this volume, figs. 2–6). These correlations are reasonable back to the late Oligocene at Site 782 and the middle Miocene at Sites 783, 784, and 786. In older sediments the correlation becomes tentative because of poor recovery and complex magnetizations (Ali et al., this volume).

Sedimentation Rates and Hiatuses

Approximate sedimentation rates can be estimated from the data yielded by Holes 782A, 784A and 786A, the sites that intersected the thickest sequences. Such preliminary figures help refine age-depth plots as presented in Fryer, Pearce, Stokking, et al. (1990). These data also suggest the presence of at least one major hiatus and perhaps several minor ones. Figures 3 through 5 give the approximate rates of sediment accumulation for Holes 782A, 784A and 786A.

Site 782 (30° 51.60′N, 141° 18.60′E; water depth, 2958 m) is located on the eastern margin of the Izu-Bonin forearc basin, northeast of the seamount Torishima (Fig. 1). The recovered 409.2 m of Eocene to Pleistocene sediments can be divided into three lithologic Subunits 1A, 1B, and 1C (Fryer, Pearce, Stokking, et al., 1990) (but not related to the subunits described for Sites 784 and 786). Subunit 1A (0–153.6 m below seafloor, mbsf) consists of Pleistocene to lower Pliocene gray to yellow-greenish, homogeneous nannofossil marl intercalated below 100 mbsf by volcanic ash layers. Subunit 1B (153.6–337.0 mbsf) is an upper Miocene to lower Miocene, light to dark gray nannofossil marl containing abundant scattered sand-sized volcanic debris. The upper Oligocene to upper Eocene interval (Subunit 1C; 337.0–409.2 mbsf) consists of vitric nannofossil chalks intercalated with tuffaceous sediment. Pebble-rich sands, gravelly conglomerates, and numerous ash layers occur near the base of Subunit 1C. Figure 3 shows the sediment age-depth plot for Hole 782A. The oldest datum used from Hole 782A (Table 1) is of late/middle Eocene age (nannoplankton Zones CP14a and CP13c), found at 390.5 mbsf. From Figure 3, three intervals during which sedimentation rates remained relatively constant can be identified. The oldest interval spans the late Eocene through late Oligocene, with a rate of roughly 3 m/m.y. During the second interval, spanning the middle and early late Miocene, the sedimentation rate increased to about 10 m/m.y and since the late Miocene, sediments have accumulated at about 29 m/m.y. This up-sequence increase in the sedimentation rate is contrary to the trend of the volcaniclastic component in the sediment, which increases overall down sequence, even though volcanic sedimentation in the form of discrete ash layers is high in the late Miocene to Holocene age interval. A significant hiatus (5 m.y.; absence of nannofossil Zones CN2 and CN3) occurs within the lower Miocene section and separates the second and third intervals of relatively constant sediment accum-ulation. In the core, the base of this hiatus is a lithologic subunit boundary delineated by a 5-cm-thick layer of manganese oxide.

As well, there is some slight evidence from the nannofossil record for a short hiatus in the upper Miocene/Pliocene succession at Site 782. This

Table 1. Biostratigraphic and magnetostratigraphic data from Hole 782A used to plot the age-depth curve in Figure 3.

Zone	Event	Core, section, interval (cm)	Depth (mbsf)	Age (Ma)	Reference (this volume)
B CN15	FO *Emiliania huxleyi*	1H-CC	9.8	0.27	Ciampo
T CN14a	LO *Pseudoemiliania lacunosa*	2H-3, 41	13.21	0.4	Ciampo
	LO *Helicosphaera sellii*	2H-CC	19.3	1.35	Ciampo
	LO *Calcidiscus macintyrei*	3H-1, 58	19.88	1.45	Ciampo
	Bruhnes S	3H-4, 100	24.8	0.73	Ali et al.
	Jaramillo S	4H-4, 130	34.6	0.98	Ali et al.
B CN14a	FO *Gephyrocapsa oceanica*	5H-2, 72	40.52	1.6	Ciampo
B CN13b	FO *Gephyrocapsa caribbeanica*	5H-6, 54	46.34	1.7	Ciampo
	Olduvai S	6H-4, 120	53.5	1.88	Ali et al.
T CN12d	LO *Discoaster brouweri*	6H-4, 121	53.51	1.88?	Ciampo
T CN12c	LO *Discoaster pentaradiatus*	7H-6, 12	64.92	2.2	Ciampo
T CN12b	LO *Discoaster surculus*	8H-5, 14	72.94	2.4	Ciampo
T CN12a	LO *Discoaster tamalis*	9H-2, 57	78.37	2.6	Ciampo
T CN11b	LO *Sphenolithus* spp.	12X-3, 82	109.12	3.4–3.5	Ciampo
T CN11b	LO *Reticulofenestra pseudoumbilica*	12X-3, 82	109.12	3.4–3.5	Ciampo
B CN11b	FO *Pseudoemiliana lacunosa*	12X-CC	115.0	3.5–3.6	Ciampo
T CN10c	LO *Amaurolithus delicatus*	13X-1, 108	116.08	3.6–3.7	Ciampo
	Cochiti E	14X-1, 140	126	3.88	Ali et al.
	Nunivak S	15X-2, 20	136	4.24	Ali et al.
B CN10c	FO *Ceratolithus rugosus*	15X-CC	139.37	4.6	Ciampo
T CN10b	LO *Ceratolithus armatus*	16X-1, 34	144.22	4.6	Ciampo
	Thvera S	16X-3, 115	148.05	4.77	Ali et al.
B CN10b	FO *Ceratolithus acutus*	16X-CC	148.16	4.6–4.8	Ciampo
T CN9b	LO *Discoaster quinqueramus*	17X-1, 92–93	54.32	5.6	Xu and Wise
B CN9b	FO *Amaurolithus primus*	21X-3, 119	196.29	6.5	Ciampo
	6N S	21X-5, 80	198.90	6.5	Ali et al.
	7BN E	23X-3, 150	216	6.85	Ali et al.
	9A E	25X-3, 130	235	7.9	Ali et al.
B CN9a	FO *Discoaster quinqueramus*	26X-2, 92–93	242.72	8.2	Xu and Wise
T CN7	LO *Catinaster coalitus*	26X-4, 92–93	245.72	9.0	Xu and Wise
T CN7	LO *Catinaster calyculus*	26X-4, 92–93	245.72	9.0	Xu and Wise
	FO *Catinaster calyculus*	26X-6, 92–93	248.72	10.0	Xu and Wise
B CN6	FO *Catinaster coalitus*	27X, 109–110	251.09	10.3	Xu and Wise
T CN5b	LO *Discoaster kugleri*	27X-3, 9–10	253.09	10.5	Xu and Wise
	5A1N E	28X-2, 70	261.80	11.55	Ali et al.
	5A2N E	29X-5, 150	276.70	12.12	Ali et al.
T CN5a	LO *Cyclicargolithus abisectus*	29X-CC	278.80	13.1	Xu and Wise
B CN5b	FO *Discoaster kugleri*	29X-CC	278.80	13.1	Xu and Wise
	5AD S	33X-4, 70	308.7	14.60	Ali et al.
T CN4	LO *Sphenolithus heteromorphus*	33X-7, 11–16	312.61	14.4	Xu and Wise
B CN4	FO *Sphenolithus heteromorphus*	35X-5, 120–121	329.70	17.1	Xu and Wise
T CN1a	LO *Reticulofenestra bisecta*	35X-6, 4–5	330.04	23.7	Xu and Wise
T CP19b	LO *Sphenolithus ciperoensis*	35X-7, 25–26	331.75	25.2	Xu and Wise
T CP19a	LO *Sphenolithus distentus*	37X-1, 61–62	342.21	28.2	Xu and Wise
T CP19a	LO *Sphenolithus predistentus*	37X-1, 61–62	342.21	28.2	Xu and Wise
B CP19a	FO *Sphenolithus ciperoensis*	39X-1, 28–29	361.18	30.2	Xu and Wise
B CP17	FO *Sphenolithus distentus*	39X-CC, 26–27	363.48	34.2	Xu and Wise
T CP16b	LO *Coccolithus formosus*	39X-CC	363.54	35.1	Xu and Wise
T CP15b	LO *Discoaster saipanensis*	40X-4, 16–17	375.16	36.7	Xu and Wise
T CP15b	LO *Discoaster barbadiensis*	40X-4, 16–17	375.16	36.7	Xu and Wise
B CP15b	FO *Istmolithus recurvus*	41X-2, 111–112	382.81	37.8	Xu and Wise
B CP15a	FO *Chiasmolithus oamaruensis*	41X-3, 60–61	383.80	39.8	Xu and Wise
T CP14b	LO *Chiasmolithus grandis*	41X-4, 42–44	385.13	40.0	Xu and Wise
B CP14a	FO *Reticulofenestra umbilica*	42X-1, 72–73	390.52	46.0	Xu and Wise

Note: T = top; B = bottom; FO = first occurrence; LO = last occurrence.

cannot be substantiated with evidence from the other fossil groups. Another possible hiatus (<1 m.y.) may be present within the lower Oligocene sequence. Evidence for the lower Oligocene hiatus again comes from the nannofossil record, but is also supported by increases in seismic velocity, density, and silica and potassium contents (Fryer, Pearce, Stokking, et al., 1990).

Site 784 (30° 54.49′N, 141° 44.27′E; water depth, 4900.8 m) is located about 4 nmi southwest of Site 783 on the lowermost, western flank of a seamount that forms part of a >500-km-long ridge along the lowermost, inner wall of the Izu-Bonin Trench (Fig. 1). The 321.1-m sedimentary sequence of at least middle Miocene to late Pleistocene age can be divided into three lithologic subunits (Fryer, Pearce, Stokking, et al., 1990). The upper Pleistocene to upper (or middle) Miocene interval (Subunit 1A; 0–126.4 mbsf) consists of vitric clayey silt and glass-rich silty clay-claystone. Subunit 1B (126.4–302.7 mbsf) consists of an upper (or middle) Miocene to middle Miocene or older vitric claystone. Subunit 1C (302.7–321.1 mbsf) comprises claystone and silt-sized serpentine of unknown age. A depleted calcareous microfossil component is a feature of Site 784, because of sediment deposition at or below the carbonate compensation depth. Figure 4 shows the sediment age-depth plot for Hole 784A. The oldest sediments dated from this hole (at 290.4 mbsf) are of middle Miocene age (based on radiolarians; see Wang, this volume). Only rare and poorly preserved nannofossil assemblages and a scattered occurrence of diatoms were found at Hole 784A, resulting in a low-resolution diatom zonation of the hole. The sedi-mentation rate at Site 784, from the late Miocene to Holocene, appears to have been relatively constant; the volcaniclastic component increases down sequence.

Site 786 (31° 52.48′N, 141° 13.58′E; water depth, 3058.1 m) is located in the centre of the Izu-Bonin forearc basin approximately

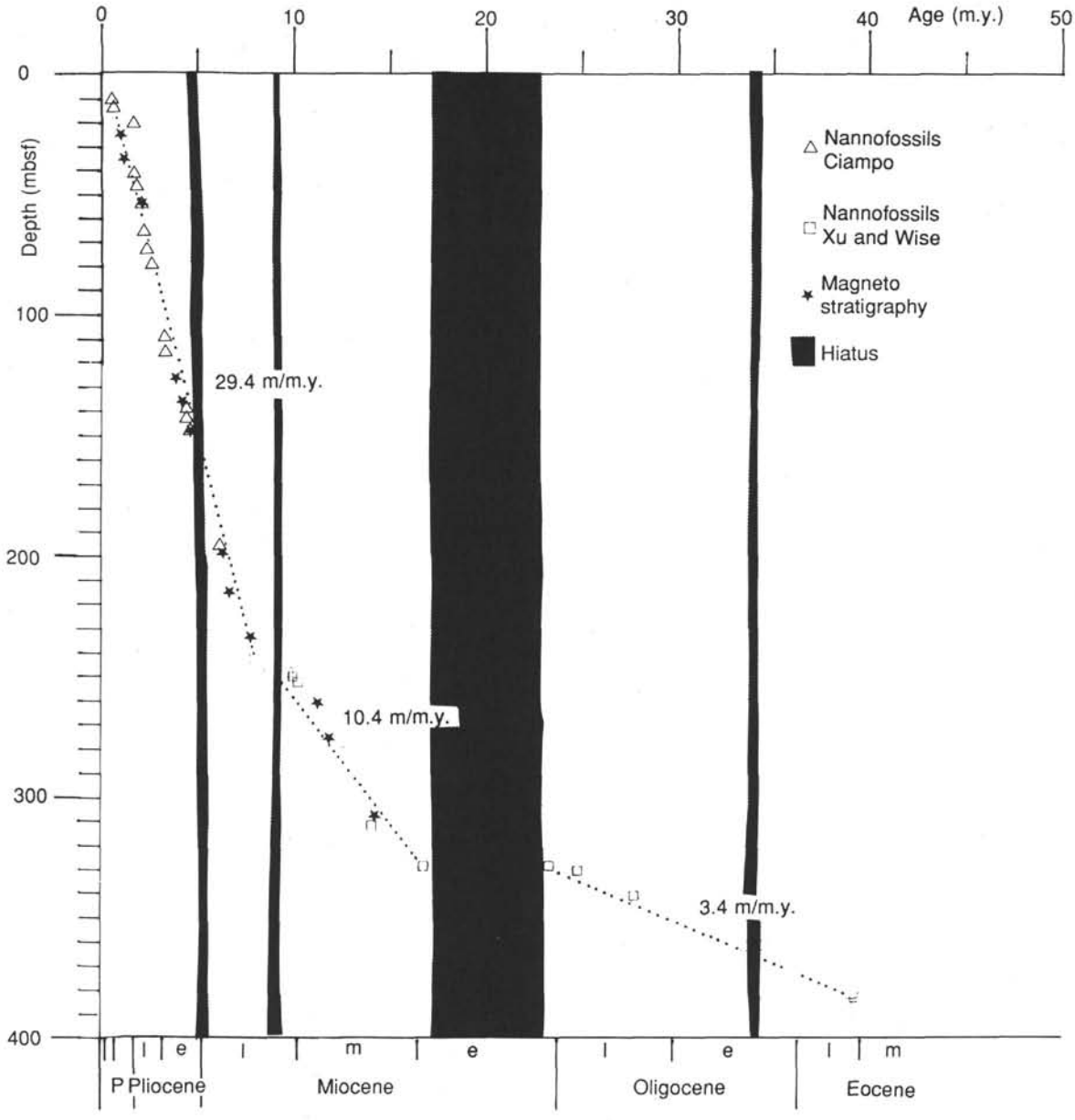

Figure 3. Age vs. depth curve for Hole 782A and estimated sedimentation rates.

120 nmi east of the active volcano, Myojin Sho (Fig. 1). The 124.90-m lower Pleistocene to middle Eocene sequence can be divided into three lithologic units (Fryer, Pearce, Stokking, et al., 1990). Unit I (0–83.46 mbsf) consists of lower Pleistocene to middle Miocene nannofossil marl and clay. Unit II (83.46–103.25 mbsf) is an upper Oligocene to middle Eocene nannofossil marl and nannofossil-rich clay. Unit III (103.25–166.5 mbsf) is a middle Eocene sequence of volcaniclastic breccia and vitric ash. Figure 5 shows the sediment age-depth plot for Hole 786A. The oldest datum used from this hole (Table 3) is of late Eocene age (nannoplankton Zone CP14), recovered from 99.6 mbsf. From Figure 4, three periods of a broadly constant rate of sediment accumulation were identified. The oldest interval spans the late Eocene through late Oligocene, where the rate was about 1 m/m.y. During the second interval, spanning the middle and early late Miocene, the sedimentation rate increased to about 4 m/m.y, whereas the later Miocene to Holocene, or third interval, sediments accumulated at about 7 m/m.y. As with Hole 782A, Hole 786A shows a similar up-sequence increase in the sedimentation rate contrary to the down-sequence trend of increasing volcaniclastic component in the succession.

At Site 786 a hiatus of about 5 m.y. is present roughly spanning the lower Miocene, based on the absence of nannofossil Zones CN2 and CN3 and a lithologic subunit boundary, represented in the core by a 10-cm-thick layer of sideromelane and manganese oxide. Shorter hiatuses within the lower Oligocene and upper Miocene/Pliocene sequences at Site 782 may be present, but cannot be recognized in Hole 786A because of the low accumulation rate for the condensed sequence in this hole (averaging 2 m/m.y.).

DISCUSSION

Holes 782A and 786A are located on the same margin of the forearc basin and contain almost identical biostratigraphic chronologies that date to the late/middle Eocene. In both holes, the hiatus previously

Table 2. Biostratigraphic and magnetostratigraphic data from Hole 784A used to plot the age-depth curve in Figure 4.

Event	Core, section, interval (cm)	Depth (mbsf)	Age (Ma)	Reference (this volume)
LO *Nitzschia reinholdii*	1R-1, 81–82	0.81	0.65	Stabell
Bruhnes S	4R-2, 50	22.40	0.73	Ali et al.
Jaramillo S	6R-5, 150	47.00	0.98	Ali et al.
LO *Rhizosolenia praebergonii*	7R-1, 23–24	49.33	1.85	Stabell
LO *Neodenticula kamtzschatica*	8R-1, 26–27	59.06	2.4	Stabell
LO *Nitzschia jouseae*	8R-4, 91–93	64.21	2.6	Stabell
FO *Rhizosolenia praebergonii*	8R-CC	68.5	3.0	Stabell
FO *Neodenticula koizumii*	9R-4, 134–135	74.34	3.2	Stabell
FO *Nitzschia jouseae*	14R-4, 48–49	121.68	4.5	Stabell
6N S	16R-7, 40	145.40	6.5	Ali et al.
7AN S	17R-5, 60	152.20	6.78	Ali et al.
7BN S	18R-5, 90	162.20	7.28	Ali et al.
LO *Thalassiosira burckliana*	21R-3, 39–40	187.79	8.0	Stabell
FO *Thalassiosira burckliana*	21R-5, 40–41	190.8	9.0	Stabell
FO *Dorcadospyris alata*	31R-CC	290.4	14.4	Wang

Note: FO = first occurrence; LO = last occurrence.

discussed is present in the lower part of the Miocene succession. This hiatus corresponds to the combined hiatuses NH1a and NH1b of Keller and Barron (1983) and recorded by them from many drill holes throughout the Pacific. Keller and Barron (1983) attributed the hiatus to intensified deep currents and increased corrosiveness of deep waters that lead to carbonate dissolution, sediment erosion, and a rise in the carbonate compensation depth. In Hole 782A, minor early Pliocene, early late Miocene, and early Oligocene hiatuses are associated with the early Miocene hiatus. The early Pliocene and early late Miocene hiatuses, hinted at by our data, correspond approximately to the widespread hiatuses NH7 and NH6 of Keller and Barron (1983), whereas the possible early Oligocene hiatus has not been noted previously in the literature and may be a local phenomenon.

The sequence recovered from Hole 786A (Holocene–middle Eocene) is greatly condensed (about 100 m of sediment compared to 385 m in Hole 782A), even though both Sites 782 and 786 are positioned similar distances from a line of active volcanoes. For both Holes 782A and 786A, sediment accumulation has increased since the late/middle Eocene (i.e., up sequence), whereas, except for an increase in ash layers in the upper Miocene to Holocene, the volcanic component within the sedimentary sequences generally decreases. This downhole increase of volcanogenic material may be a result of high volcanic influx in the Eocene/Oligocene, from a postulated volcano, or volcanoes, nearby.

Following the early Miocene hiatus a sharp, relative increase in the rate of sediment accumulation occurs, with another increase during the late Miocene. The second increase in the rate of sediment accumulation in the late Miocene probably reflects the combined input of increased biogenic and volcanogenic sediment. Fryer, Pearce, Stokking, et al. (1990) noted numerous discrete ash layers in the upper Miocene to Holocene sediments of Holes 782A and 786A, reflecting a renewed increase in volcanicity. The presence of discrete ash layers in the upper Miocene to Holocene sediments may reflect a more distant source, in contrast to the volcaniclastic breccias and ubiquitous volcanic glass present throughout the Eocene/Oligocene sediments.

Hole 784A, although farther east than Holes 782A and 786A and containing a younger middle Miocene basement, shows a sedimentation pattern and rate similar to that of Hole 782A.

CONCLUSIONS

Data from the use of nannofossils, radiolarians, foraminifers, and diatoms has established a biostratigraphic framework ranging from middle Eocene to Holocene, with gaps that suggest corresponding sedimentary hiatuses in the early Oligocene (possible), early Miocene (likely), and two in late Miocene and earliest Pliocene, respectively;

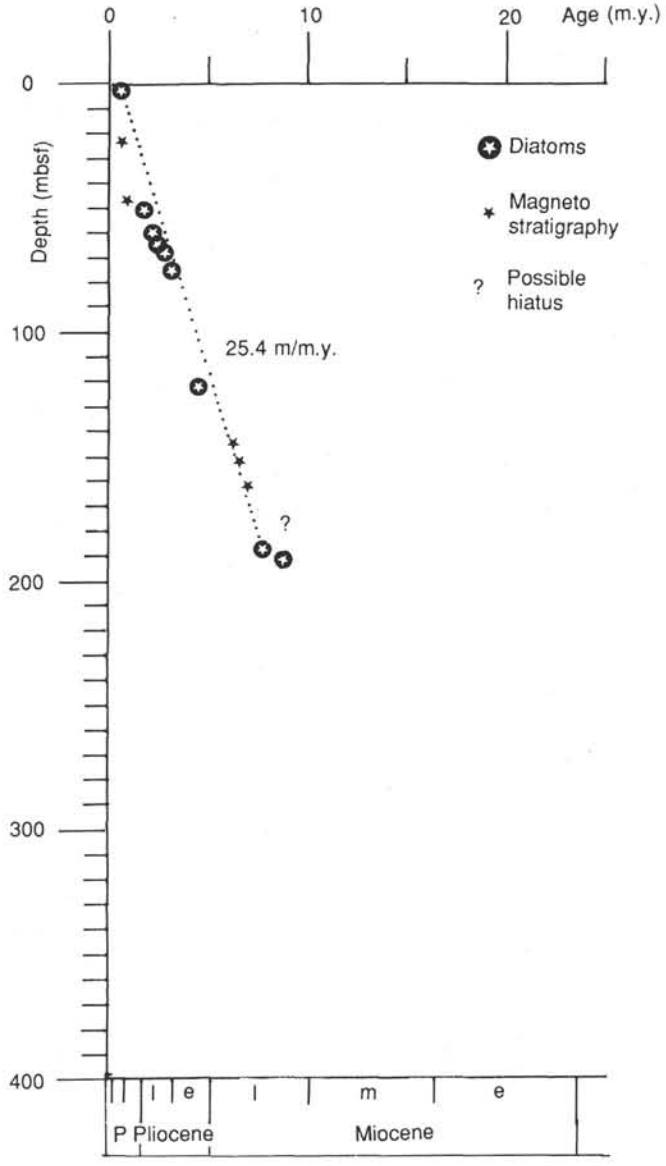

Figure 4. Age vs. depth curve for Hole 784A and estimated sedimentation rates.

the last two are suspect. The zonation schemes from all of these fossil groups correspond closely. Sediment accumulation varies from hole to hole (e.g., in Hole 786A the suggested rate of sediment accumulation for the late Miocene to Pleistocene is lower than for the same time period in Hole 782A). It must be noted that these figures are approximations, but the important observation is that the slopes shown in Figures 3, 4, and 5 are comparable, with the fastest rates for the late Miocene to Holocene and the slowest rates present in the middle Eocene to late Oligocene.

Increased sedimentation rates during the late Miocene to Holocene may have resulted from increased volcanic sediment input. The location and source of the volcanic materials, especially those in Holes 782A and 786A, are uncertain.

REFERENCES

Akiba, 1986. Middle Miocene to Quaternary diatom biostratigraphy in the Nankai trough and Japan trench, and modified lower Miocene through Quaternary diatom zones for middle-to-high latitudes of the North Pacific. *In* Kagami, H., Karig, D. E., Coulbourn, W. T., et al., *Init. Repts. DSDP,* 87: Washington (U.S. Govt. Printing Office), 393–481.

Table 3. Biostratigraphic and magnetostratigraphic data from Hole 786A used to plot the age-depth curve in Figure 5.

Zone	Event	Core, section, interval (cm)	Depth (mbsf)	Approximate age (Ma)	Reference (this volume)
CN14a		1H-1, 2	0.02	1.6–1.45	Ciampo
CN13b		1H-1, 50	0.50	1.7–1.6	Ciampo
CN12b		1H-2, 96	2.46	2.6–2.4	Ciampo
T CN12a	LO *Discoaster tamalis*	1H-3, 96	3.96	2.6	Ciampo
	Matuyama S	1H-3, 15	4.65	2.47	Ali et al.
	Gauss E	2H-6, 60	17.60	3.18	Ali et al.
B CN12a	FO *Discoaster tamalis*	2H-CC	19.2	3.4–3.5	Ciampo
T CN10c	LO *Amaurolithus delicatus*	3H-1, 85	20.05	3.6–3.7	Ciampo
B CN10c	FO *Ceratolithus rugosus*	4X-CC	30.88	4.6	Ciampo
T CN9b	LO *Discoaster quinqueramus*	5X-1, 132	39.52	5.6	Ciampo
T CN9b	LO *Discoaster berggrenii*	5X-1, 132	39.52	5.6	Ciampo
B CN9b	FO *Amaurolithus primus*	5X-2, 26	39.96	6.5	Ciampo
B CN9a	FO *Discoaster quinqueramus*	5X-CC	47.6	8.2	Xu and Wise
B CN9a	FO *Discoaster berggrenii*	5X-CC	47.6	8.2	Xu and Wise
T CN7	LO *Catinaster calyculus*	6X-1, 51–52	48.12	9.0	Xu and Wise
	FO *Catinaster calyculus*	6X-2, 70	49.80	10.0	Xu and Wise
T CN4	LO *Sphenolithus heteromorphus*	8X-1, 35–36	67.46	14.4	Xu and Wise
B CN4	FO *Sphenolithus heteromorphus*	9X-5, 57–58	83.37	17.1	Xu and Wise
T CN1a	LO *Reticulofenestra bisecta*	9X-5, 62–63	83.42	23.7	Xu and Wise
T CP19b	LO *Sphenolithus ciperoensis*	9X-5, 80	83.60	25.2	Xu and Wise
B CP19a	FO *Sphenolithus ciperoensis*	10X-3, 14–15	89.55	30.2	Xu and Wise
T CP16b	LO *Reticulofenestra umbilica*	10X-4, 14–15	91.04	34.6	Xu and Wise
T CP15b	LO *Discoaster saipanensis*	11X-1, 8–10	96.70	36.7	Xu and Wise
T CP15b	LO *Discoaster barbadiensis*	11X-1, 8–10	96.70	36.7	Xu and Wise
T CP15b	LO *Chiasmolithus oamaruensis*	11X-1, 8–10	96.70	36.7	Xu and Wise
B CP15b	FO *Isthmolithus recurvus*	11X-2, 62–63	98.12	37.8	Xu and Wise
B CP15a	FO *Chiasmolithus oamaruensis*	11X-2, 70	98.20	39.8	Xu and Wise
T CP14b	LO *Chiamolithus expansus*	11X-3, 58–59	99.59	40.0	Xu and Wise

Note: T = top; B = bottom; FO = first occurrence; LO = last occurrence.

Barron, J. A., 1985a. Miocene to Holocene planktonic diatoms. *In* Bolli, H. M., Saunders, J. B., and Perch-Nielsen, K. (Eds.), *Plankton Stratigraphy:* Cambridge (Cambridge Univ. Press), 763–809.

————, 1985b. Diatom paleoceanography and paleoclimatology of the central and eastern equatorial Pacific between 18 and 6.2 Ma. *In* Mayer, L., Theyer, F., Thomas, E., et al., *Init. Repts. DSDP,* 85: Washington (U.S. Govt. Printing Office), 935–945.

Berggren, W. A., and Miller, K. G., 1988. Paleogene tropical planktonic foraminiferal biostratigraphy and magnetobiochronology. *Micropaleontology,* 34:362–380.

Blow, W. H., 1969. Late middle Eocene to Recent planktonic foraminiferal biostratigraphy. *In* Brönniman, P., and Renz, H. H. (Eds.), *Proc. First Int. Conf. Planktonic Microfossils,* Geneva, 1967. Leiden (E. J. Brill), 1:199–422.

————. 1979. *The Cainozoic Globigerinida:* Leiden (E. J. Brill).

Fryer, P., Pearce, J. A., Stokking, L. B., et al., 1990. *Proc. ODP, Init. Repts.,* 125: College Station, TX (Ocean Drilling Program).

Keller, G., and Barron, J. A., 1983. Paleoceanographic implications of Miocene deep-sea hiatuses. *Geol. Soc. Am. Bull.,* 94:590–613.

Kennett, J. P., and Srinivasan, M. S., 1983. *Neogene Planktonic Foraminifera: A Phylogenetic Atlas:* Stroudsburg, PA (Hutchinson Ross).

Okada, H., and Bukry, D., 1980. Supplementary modification and introduction of code numbers to the low-latitude coccolith biostratigraphic zonation (Bukry, 1973; 1975). *Mar. Micropaleontol.,* 5:321–325.

Sanfilippo, A., Westberg-Smith, M. J., and Riedel, W. R., 1985. Cenozoic radiolaria. *In* Bolli, H. M., Saunders, J. B., and Perch-Nielsen, K. (Eds.), *Plankton Stratigraphy:* Cambridge (Cambridge Univ. Press), 631–712.

van Andel, T. H., Heath, G. R., and Moore, T. C., Jr., 1975. *Cenozoic History and Paleoceanography of the Central Equatorial Pacific. A Regional Synthesis of Deep Sea Drilling Project Data.* Mem. Geol. Soc. Am., 143.

Date of initial receipt: 10 December 1990
Date of acceptance: 28 June 1991
Ms 125B-169

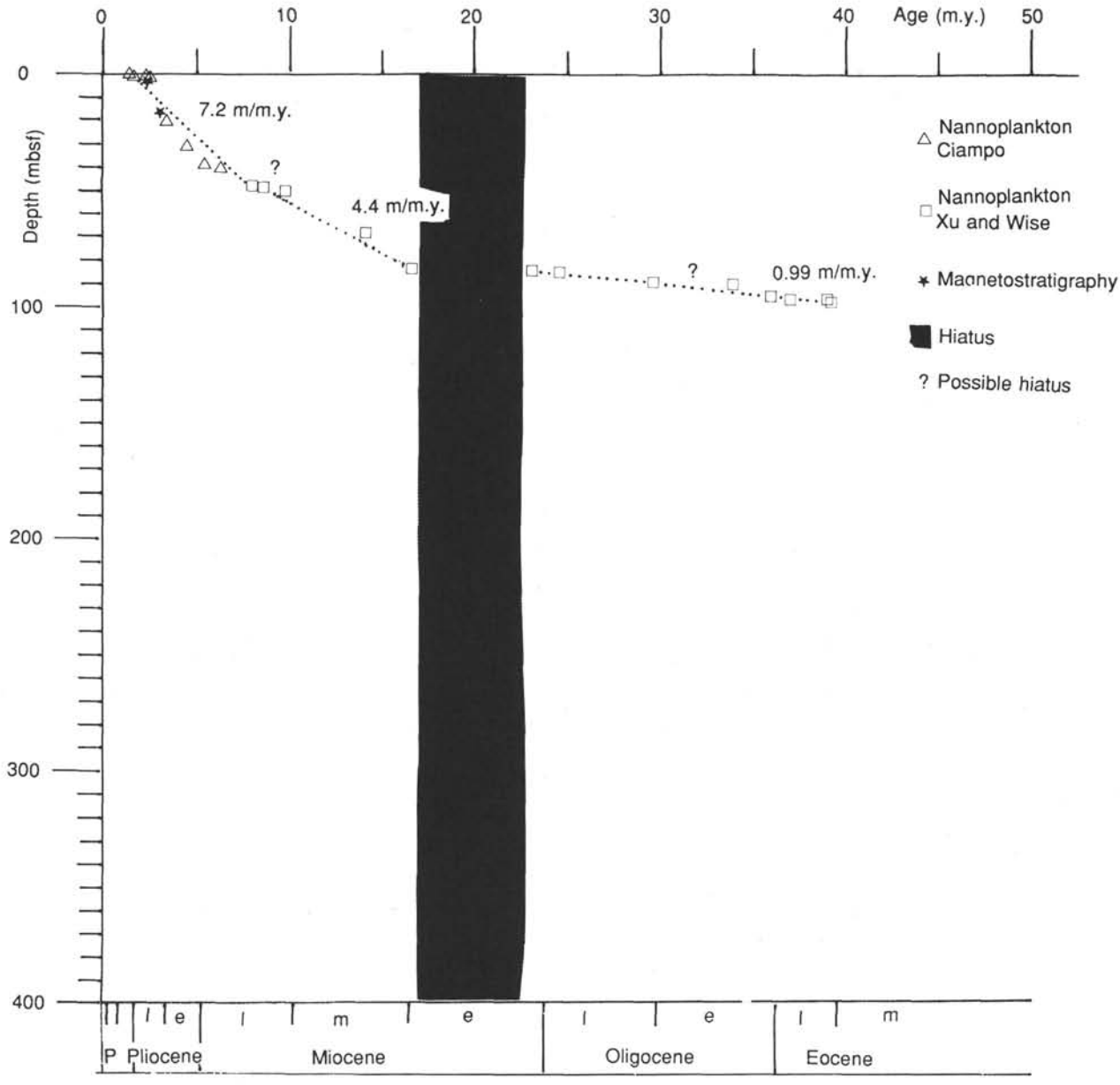

Figure 5. Age vs. depth curve for Hole 786A and estimated sedimentation rates.